

The Effect of Stirring Rate on Electrodeposition of Nanocrystalline Nickel Coatings and their Corrosion Behaviors and Mechanical Characteristics

Kaveh Rahimi Mamaghani, Seyed Morteza Naghib*

Department of Nanotechnology, School of New Technologies, Iran University of Science and Technology (IUST), Tehran, Iran

*E-mail: Naghib@iust.ac.ir

Received: 25 February 2017 / Accepted: 19 April 2017 / Published: 12 May 2017

Nanocrystalline pure nickel coating was electroplated on pure copper by means of a modified Watts bath with variant stirring rates and current densities. The crystallite sizes were calculated by XRD analysis. The crystallite size had an inverse relation with stirring rate and current density in the plating bath. The best corrosion resistance was observed in 5 A/dm² current density of polarization test and corrosion rate smoothly increased by agitation in the plating bath. The microstructure evolution at high stirring rates exhibited some surface bubbles that affected the surface quality and properties. Although Vickers microhardness increased by the addition of the current density, our measurements showed that the hardness had an inverse relationship with turbulence in the solution. An optimum agitation in the bath could improve the hardness distribution on the coated specimen. However, specimens with agitation did not follow the Hall–Petch relationship between crystallite size and microhardness.

Keywords: Nanocrystalline nickel; Electrodeposition; Stirring rate; Corrosion; Hardness.

1. INTRODUCTION

Nowadays, interests in investigating nanocrystalline coatings are rapidly increasing among researchers. It has been noticed before that mechanical property of nanocrystalline coatings is excessively depended on its structure and particle size [1-3]. There are many features like high-end quality, perfect possession on the process which make electroplating a unique method to manufacture coatings for various metallurgical or biomaterial applications [4-6]. These benefits granted electroplating a preponderance which spread this method worldwide for depositing nickel on various substrates. Moreover, by utilization of nano-sized nickel particles the mechanical properties of the coating could be boosted to higher levels [7-10]. As known, the corrosion resistance of a coating is an essential factor in weighing the quality of the coatings [11]. Recently, researchers have reported that

nano-structure nickel coatings demonstrate better corrosion resistance than ordinary bulk nickel coatings [12, 13]. Also, Mishra et al [14] presented curves that show the active-passive current behavior of nickel layer according to the potential changes and illustrated that freshly exposed nanocrystalline nickel has more corrosion resistance than bulk one indicating higher impediment to anodic dissolution from the nanocrystalline nickel. Improved corrosion resistance could be obtained by changing the orientation and size of the crystallite. In order to achieve nanoscale nickel particles, the nucleation rate should be significantly much more than the growth rate of the particles. Accordingly, to escalate nucleation rate and reduce growth rate factors like negative over-potential ion density nearby the cathode and ionic surface mobility should be ameliorated [15, 16]. Previous research demonstrated that high current density is a particular solution to refine the structure of coating in order to achieve nano-structured coating [17]. According to the literature, the logarithm of the system current density has a linear relationship with the logarithm of the coating crystallite size [8, 18-20]. Although, there is an optimum point that further enhancement in the current density results in an opposite effect. Increasing the current density leads to crystallite size enlargement since the concentration reduction of nickel ions in the electrolyte nearby the coating surface that reduces the nucleation rate [21, 22]. Furthermore, electrodeposition parameters at the cathode surface have a significant effect on the process of coating forming [18, 23, 24]. Rashidi et al [6] electrodeposited nickel coating in a Watts bath with 5 g/l saccharin by applying 7.5 A/dm² direct current density. It was reported that crystallite size reduced to 24nm. Meanwhile, new researchers developed that cathode type, current density, and concentration of the plating bath additives are imperative parameters in modifying the nickel coatings structure and crystallite size [24-27]. The effect of temperature on the nickel-coated materials can be found in these references [28-30]. Rasmussen et al [29] found that temperature and current density have a limited effect on the hardness and microstructure of the deposited bulk nickel layers. Other report showed that the temperature had negligible influence on the nucleation rate and nanocrystalline size of nickel coatings [27].

Likewise, agitation is a key system factor that has a compelling effect on crystallite size and it can hamper the crystal growth leading to finer crystallite size. Moti et al [31] set up a copper cylinder electrode in watts bath containing saccharin. They reported that enhancement in the electrode rotation speed increased the saccharin adsorption that caused more diminution in the crystallite size. Increasing saccharin concentration causes to decrease the crystallite size of nickel coating. However, concentrations beyond 3 g/l have no effect on the microstructure of coatings [26, 27]. Meanwhile, a set of spherical specimens on a rotating cathode in ammonium nickel sulfate and nickel chloride bath resulted in a glossy nickel coating [32]. Benea et al [33] expressed that increasing the rotation speed would easily remove the corrosion products from the surface leading to activation of the coating surface. Also, mechanical and physical properties of nickel coating could be optimized by increasing the saccharine in the bath [14]. Decreasing nanocrystalline size would notably increase the nickel coating hardness. However, the increasing of hardness rate slows down by further decreasing of nanocrystalline size [9]. Nieh et al [34] demonstrated a hall-petch breakdown in nano nickel coating with 14 nm grain size by using nanohardness and nanoscratch experiments. There was a microhardness variation as stated in the Hall-Petch equation in nanocrystalline size beyond 10 nm. Also, other work showed the highest hardness was conducted at 55°C [20]. Nanocrystalline nickel coating was

electrodeposited using current pulse by Wang et al in 2006 that might not be suitable for industrial applications [35].

The direct current is the most prevalent method in the coating industry. Therefore, in this research producing a bright nanocrystalline pure nickel coating has been considered by this method with desirable properties. In order to modify mechanical and corrosion properties, the effect of stirring rate on these materials has been investigated for the first time. Moreover, in favor of optimizing the process efficiency, reasonable low range current density was applied. The most previous efforts [36-39] have discussed stirring rate effects on coatings qualities and have investigated the influence of stirring rate with some other particles (named nanocomposite with particles smaller than 100nm) and have demonstrated that the stirring rate has a significant effect on these particles dispersion. In other words, it was proved that higher stirring rate enhanced the percent of nanoparticles and the trend of the weight percent justifying by collision factor [40, 41]. On the other side, in previous reports, the process has been done by the pulse current although the use of direct current is so common in the industry. They also never mentioned the variation of microhardness distribution and hardness inhomogeneity of coating surface. In this work which is focused on pure nickel coatings that are more common and cheaper material in industrial productions, the effects of stirring rate on microhardness, microstructure, corrosion rate, and crystallite size were investigated.

2. EXPERIMENTAL

The pure copper is a common substrate to study of nickel electroplating. Definitely, structural compatibility between nickel and copper improves the adhesion of electrodeposition. Nanocrystalline pure nickel coating was prepared in a modified Watts bath containing nickel sulfate as the main source of nickel ions (Merck, 99%) 240 g/l, nickel chloride to increase dissolution (Merck, 98%) 30 g/l, boric acid as buffering agent (Merck, 99.8%) 30 g/l, and some surfactants like Saccharine 10g/l (Merck 99%) were added as grain refining agent. The bath pH was controlled to be about 4.0 and a double distilled water was used to prepare the solution. Preparation steps before electroplating were: 1- rinsing all samples with an alkali solution, 2- draining the sample, 3- activating the samples in a 10% sulfuric acid, 4-rinsing the samples and transferring them to the bath. The total time of the deposition was 30 min. In order to achieve fine crystalline structure, all experiments were performed at a constant temperature, 55°C, [20] with direct current. The electroplating process was performed in a 1000 ml electrolyte applied parallel electrodes. A piece of nickel with $80 \times 40 \times 10 \text{ mm}^3$ dimensions as the anode and a part of copper with $80 \times 30 \times 1 \text{ mm}^3$ dimensions was applied as the cathode. The whole experimental process divided into two stages. In the first stage, there was no turbulence in the bath and current densities 3, 5, 7 and 9 A/dm² were applied by DC power supply. In the secondary stage, the optimal current density found to be 5 A/dm² was used. The bath stirring rates were 100, 200, 300, 400 and 500 rpm that agitated by a magnetic stirrer in the center of the solution. At the end, all specimens are cleaned and washed with alcohol for the characterization.

X-ray diffraction (XRD) patterns were used to determine the crystallite size of coated samples. XRD measurements were carried out on a Philips Holland X'Pert PW 3040/60 X-ray diffract meter

using CuK α radiation with a step width of 0.02°. In order to calculate the crystallite size of specimens the X'pert High Score software was used with calculations according to the Scherer equation. The equation is as follows:

$$d = \frac{k\lambda}{B \cos \theta} \tag{1}$$

Where d is the crystallite size, B is the full-width at half-maximum (FWHM), θ is the Bragg's angle, λ is the wavelength and k is the Scherer constant which is equivalent to 0.9. A full annealed nickel specimen with an average grain size of 40 μm was also applied for correcting instrumental peak broadening. FWHM of the specimen (B_{exp}) was calculated with the following Gaussian equation used to minimize the device FWHM (B_{ins}) [3].

$$B^2 = B_{\text{exp}}^2 - B_{\text{ins}}^2 \tag{2}$$

The morphology and microstructure of coatings were investigated using scanning electron microscopy (S360, Cambridge Instruments). Electrochemical properties and corrosion behavior of the prepared coatings were studied by polarization test that was applied at ambient temperature in a solution of 3.5 wt% NaCl according to ASTM B117 standard at a sweep rate of 1 mV/s. The Vickers microhardness was taken on a polished surface of samples using a Buehler microhardness tester with applied load of 30 gf for 10 s (according to the ASTM E384 standard). The final microhardness values were the average of 10 measurements performed through the length of the coated specimens.

3. RESULTS AND DISCUSSION

3.1. Crystallite size

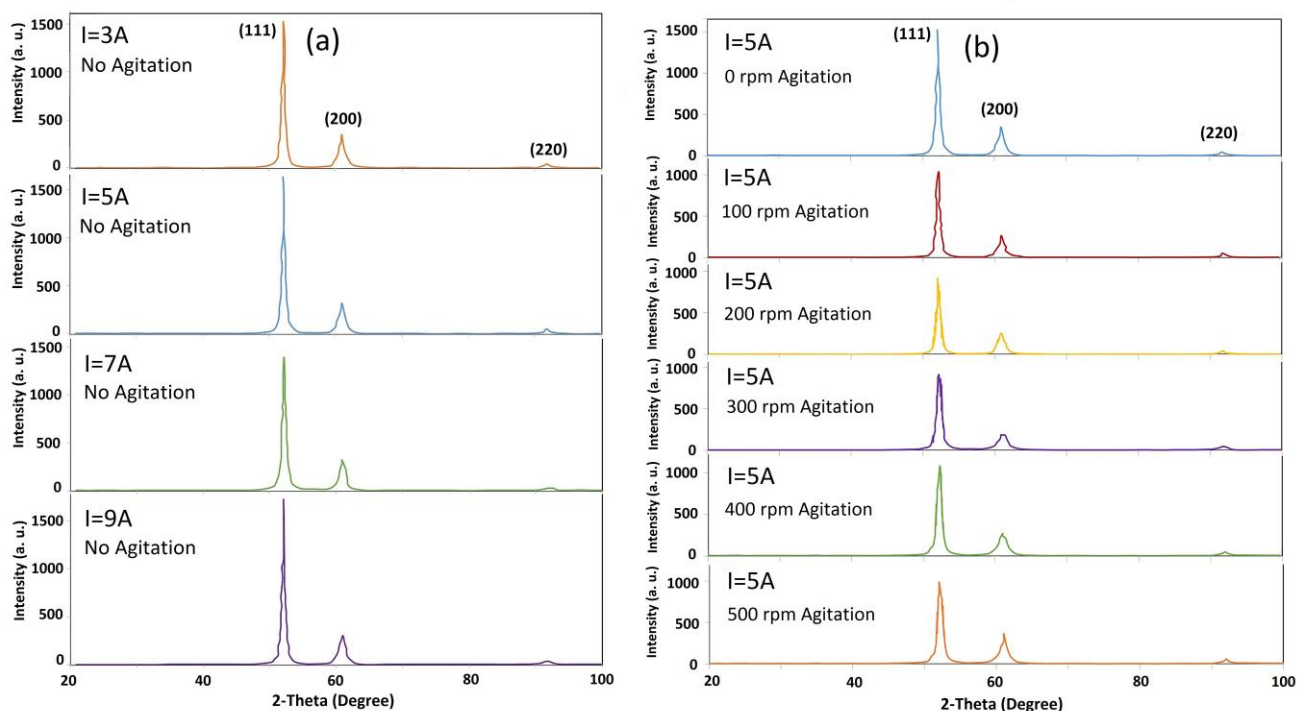


Figure 1. XRD patterns of prepared nickel coating samples at different current densities (a) and stirring rates (b).

The XRD results of nickel coatings were shown in Figs. 1(a) and 1(b). In Fig. 1(a) the electrolyte solution was static with different current densities and in Fig. 1(b) the electrolyte solution had agitation at different rates in a constant current density. The crystallite sizes were calculated by using Scherer formula in (111) peak which is the strongest preferred orientation in FCC materials.

The variations of coating crystallite size were shown in Fig. 2. The results of coating crystallite size in Fig. 2(a) indicated that the higher current density decreased the size of nickel crystallites. This phenomenon was reported in previous researches [6, 9, 42]. Theoretically, these results were predictable because increasing the current density leads to increase the polarization and the nuclear generation rate which ultimately led to the formation of finer crystallites. The similar behavior can be found in Fig. 2(b). The decreasing of crystallite size was observed with increasing the turbulence in the system because increasing the turbulence has acted as a deterrent for developing large crystals by the formation of nickel atoms community. Also increasing the turbulence could create better additive adsorption on the surface that led to improving the crystalline microstructure [31]. The related manuscripts in this research area [36-39] mentioned that adding reinforcements like CeO₂ particles could improve the mechanical properties and corrosion resistance although the effect of the as-synthesized CeO₂ particle size on the final Ni-CeO₂ nanocomposite crystallite size was not considered. However, in this research, the crystallite size in optimum conditions was 28 nm which was lower than the crystallite size previously reported in the literature [36]. Therefore, it seems that adding nanoparticles as reinforcement to the nickel coating might not always have a significant effect in electrodeposited crystallite size refinement. In other words, manipulating the other process parameters (without adding nanoparticles) could help easier manufacturing, better control, and lower production cost.

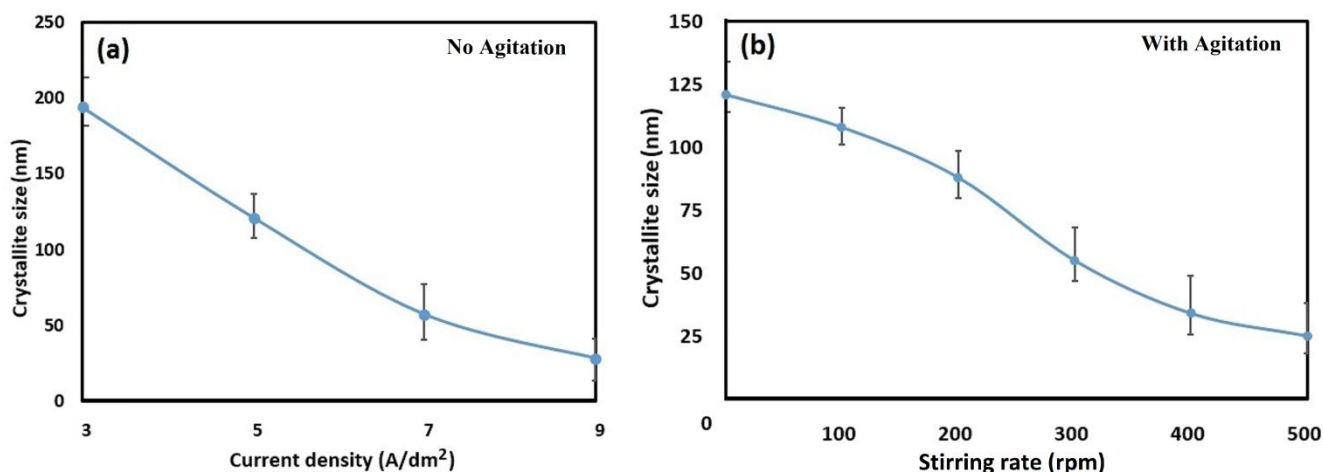


Figure 2. Variation of nickel coatings crystallite size: (a) at different current densities in the stationary bath (stirring rate = 0 rpm), (b) at 5 A/dm² current density with different stirring rates.

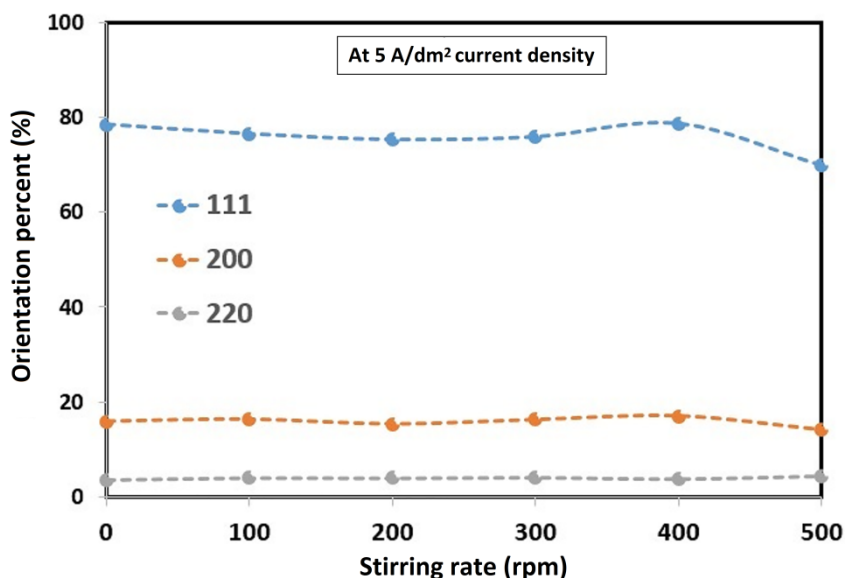


Figure 3. Variation of (111), (200) and (220) orientations percent at 5 A/dm² current density with different stirring rates according to the XRD peaks.

According to XRD patterns, the crystal planes corresponding to each diffraction peak were (111), (200) and (220). Each orientation percent was calculated according to the intensity ratio of the specific peak achieved by the sum of all peaks intensities. The orientation percent of all samples with rotational bath are shown in Fig. 3. Indeed, the higher stirring rate in the bath decreased the (111) orientation percent slightly and (220) and (200) orientation percent were opposite. A sudden decrease in (111) orientation percent of 500 rpm sample and the microstructure observations indicated that the increase of bath rotational speed could enhance the polishing of coating surface and cause opposite trend for the crystal orientation degree.

3.2. Microstructure

Scanning electron microscopy was used to measure surface morphology and quality. Figs. 4(a) and 4(b) showed a network of crack on the coating. Fig. 4(b) demonstrated some blisters on the network of cracks. The specimen in Fig. 4(c) had the maximum stirring rate. It can be figured out from the image that the specimen had a relatively homogenous structure which consisted of very fine crystallites and some bubbles with average size about 100 nm diameters were also found. It seems that high agitation in the bath caused to remain these bubbles on the nanocrystalline pure nickel coating. Maybe, these hollow like bubbles were hydrogen blisters (as a slight shift of the main pick of nickel (111) absorbed in XRD results) related to microstrains brought hydrogen uptake during the deposition process. The sphere-like bubbles could be considered in previous works as some added nanoparticles in nanocomposite coatings (especially sphere like ones). This may be the most reason that these bubbles were not highlighted before in high stirring rates.

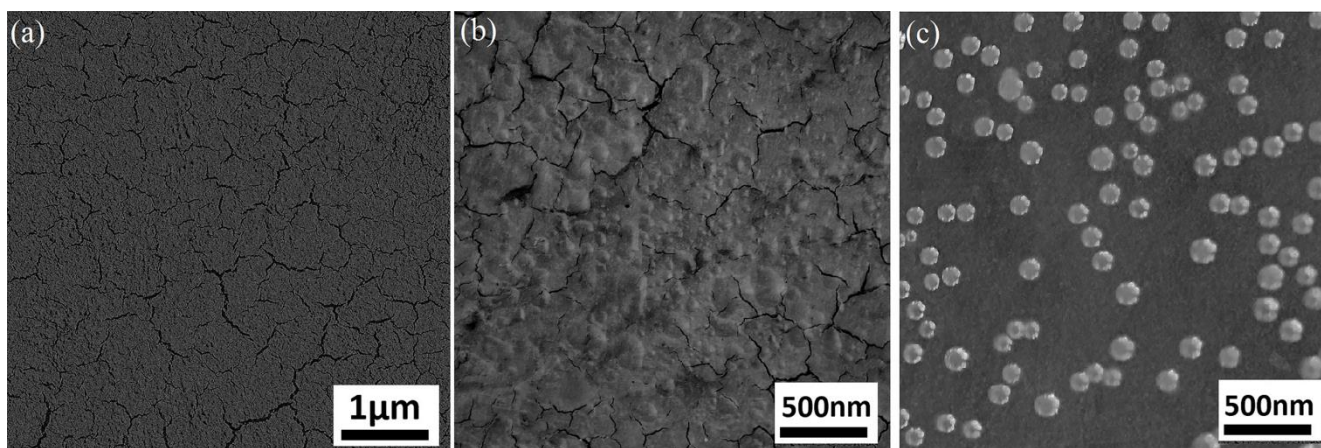


Figure 4. SEM images of prepared nickel coatings at 5 A/dm² current density. (a) without agitation, (b) with 300 rpm and (c) with 500 rpm stirring rates in the solution.

3.3. Corrosion

The effects of static and dynamic states on the polarization curves of nanocrystalline pure nickel coatings were presented in Figs. 5 (a) and (b), respectively. The corrosion current density was calculated in the range of E_{Corr} ±10 mV according to Stern-Geary equation [43]. The values of β_a and β_c were assumed equally as 0.12V which is an acceptable estimate for the values of anodic and cathodic Tafel.

$$I_{corr} = \frac{I_{appl}}{2.303 \Delta\phi} \left(\frac{\beta_c \beta_a}{\beta_c + \beta_a} \right) \tag{3}$$

Where, Δφ / I_{appl} is the slope of polarization in the region near corrosion potential that Δφ has a linear relation with the I_{appl}. The Δφ / I_{appl} amount is equal to the polarization resistance of specimens defined as R_p. Moreover, the β_a and β_c are the anodic and cathodic Tafel constants. The value of Δφ could not be more than 10 mV in a partial polarization. The electroplating conditions did not affect the cathode surface and the ratio of anode surface to the cathode surface.

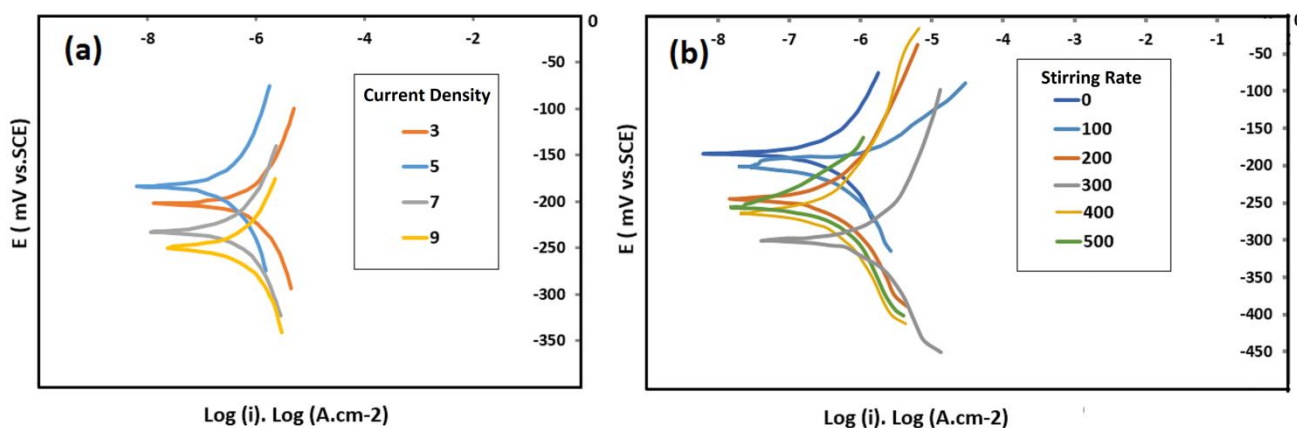


Figure 5. Polarization curves of prepared Ni coatings in 3.5% NaCl solution at (a) different current density with no agitation condition, (b) different stirring rates with 5 A/dm² current density.

The calculated results from Fig. 5 containing potentials and current densities of corrosion, Tafel slopes, and polarization resistances were demonstrated in table 1. The determined optimum current density with the best corrosion resistance was 5 A/dm². Therefore, the effect of electrolyte stirring rate was scrutinized for this amount of current density. This current density was also approved as the optimum current density for depositing nanocrystalline nickel coating by Zhao et al. [44]. Increasing the current density primarily resulted in decreasing the crystallite size and secondly led to increasing the current density of corrosion.

The additives in the bath decreased the formation of hydrogen bubbles stuck to the cathode and minimized the waste consumption of hydrogen ion which resulted in a more efficient deposition process. Furthermore, particles on the cathode surface e.g. can behave like an anti-actuator and deposit on the crystallite boundaries acting as a surface producer [45]. In order to hamper the sedimentation of hydroxide, commercial additives were solved in the solution. These additives could be beneficial in increasing the corrosion resistance of the coating. On the other side, it could be argued that increasing the current density leads the structure to the finer crystallite size that causes an accretion in the crystallite boundary density. This crystallite boundaries enhancement could be harmful if no inactive layers persist on them, so it might end with an increase in the corrosion rate of the coating surface. The β_c values (in table 1) did not change significantly in all specimens. However, the β_a value enhanced with a higher stirring rate that may be related to the coating porosities (Fig. 4) and a more available surface, leading to the higher anodic reactions and steep slope.

It can be figured out from the polarization test that increasing the stirring rate concluded finer crystallite size and upper stirring rate led to higher corrosion current density and corrosion rate. Fig. 5(b) demonstrates the effect of stirring rate on corrosion behavior of coating which indeed increasing the stirring rate had a conflicting result on crystallite size and corrosion rate. In table 1, it is clear that in higher applied current densities and intense stirring rates the corrosion potential was shifted to more negative values. Between the different stirring rates, the highest R_p value calculated with Stern-Geary formula were obtained at 400 rpm which was equal with the no agitation specimen. This result indicated a little effect of agitation on corrosion properties of the samples. Also, the discussed trends did not see at 500rpm so there is an optimum point in stirring rate variations of this process. In similar works, R. Sen [36] reported that the presence of some particles like CeO₂ could amplify corrosion rate in higher stirring rate (550 rpm). However, in our work (pure nickel coatings), there was not a significant change in the corrosion rate of the samples that may be related to the bubbles. Fig. 4(c) also proved the formation of bubbles stuck into the cathode surface (sample).

Table 1. The results of polarization test for all samples in different conditions of current density and stirring rate.

E_{corr} vs. SCE (mV)	I_{corr} ($\mu\text{A}/\text{cm}^2$)	Stirring rate (rpm)	Current density (A/dm^2)	β_a (mV/decade)	β_c (mV/decade)	R_p from Tafel ($\text{k}\Omega.\text{cm}^2$)
-249	0.8078	0	9	151.1	211.4	47.7
-232	0.7942	0	7	186.4	158.4	46.8
-184	0.3981	0	5	195.3	193.5	106

-202	0.4266	0	3	157.7	177.1	84.9
-201	0.5062	100	5	182.6	205	82.8
-245	0.5158	200	5	225.9	203.3	90.1
-300	0.5747	300	5	328.9	198.6	93.6
-264	0.5383	400	5	365.7	205.1	105.9
-256	0.5831	500	5	154.6	204.35	65.5

3.4. Mechanical properties

There are many ways to characterize the mechanical properties of a coating but the most common way is measuring the hardness of the coating. Microhardness would be an outstanding method for measuring the hardness of nanocrystalline coatings. Microhardness test results revealed that decreasing crystallite size caused a significant boost of microhardness although these changes slowed down with further decreasing in crystallite size [9]. The synthesized nanocrystalline nickels microhardness was fourth times higher than annealed bulk nickel (around 600 HV). As shown in Fig 6, the same results were observed in a non-rotational bath at various current densities. This figure disclosed that increasing current density caused higher microhardness values.

This manuscript examines the development of microhardness inhomogeneity factor in nano nickel coatings at elevated stirring rates. In order to quantify the inhomogeneity in the coated samples, inhomogeneity factor is defined as:

$$I.F. = \frac{\sqrt{\frac{\sum_{i=1}^n (H_i - H_{ave})^2}{(n-1)}}}{H_{ave}} \times 100 \tag{4}$$

Where H_i denotes the hardness value of i -th measurement, n is the number of hardness measurements on each coated specimen and H_{ave} is the mean hardness value. In general, the less I.F. value indicates higher homogeneity of mechanical properties.

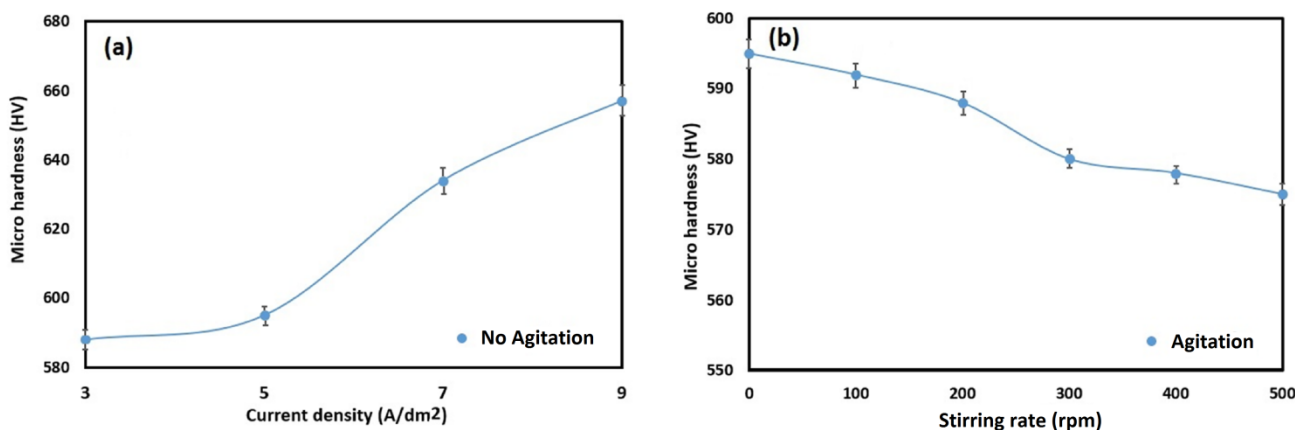


Figure 6. The Vickers microhardness value at different current densities without agitation in the solution (a) and at different stirring rates in the solution (b).

The microhardness distribution through samples and results of inhomogeneity factor were shown in Figs. 7 (a) and (b). Inhomogeneity factor variations demonstrated that the microhardness homogeneity was increased in higher stirring rates. In other words, the microhardness became more homogeneous with higher stirring rates. By contrast, it is clear that the homogeneity was efficiently limited after 400 rpm stirring rate. This result verified that the inhomogeneity was developed through higher speeds (like 500 rpm). It has been reported [46] that the solution bath stirring by rotational cathode could change the thickness of the coating in different sections investigations. The study on coatings thickness of all specimens showed no makeable alterations. As discussed before, microstructure investigations and these results indicated that the nickel coatings required an optimized stirring rate to achieve an equilibrium structure of nanoscale crystallites. R. Sen [36] reported that the Ni-CeO₂ coatings had an optimum stirring rate for their hardness property at 450 rpm. However, their hardness variations with stirring rate were different with this work that may have come from CeO₂ particles presence in their solution bath.

Similar microhardness results have been reported by means of the conventional Hall-Petch relationship in previous studies [42, 43, 45]. This equation is as followed:

$$H_v = H_0 + K_H \cdot d^{-1/2} \tag{5}$$

Where H_v is the measured hardness and parameter d indicates the crystallite size. Constants H_0 and K_H depend on hardness measurement conditions. It can be concluded from this equation that finer crystallite size led into higher hardness values. This intensification can be explained by an increase in total area of crystallite boundaries. Finer crystallite size increased the ratio of total area of crystallite boundaries in a unit volume which intensified the barriers against dislocations motion and finally augmented the hardness of the material. Figs. 8 (a) and (b) also implied this theory and showed that the results were identical with anticipations of the Hall-Petch equation.

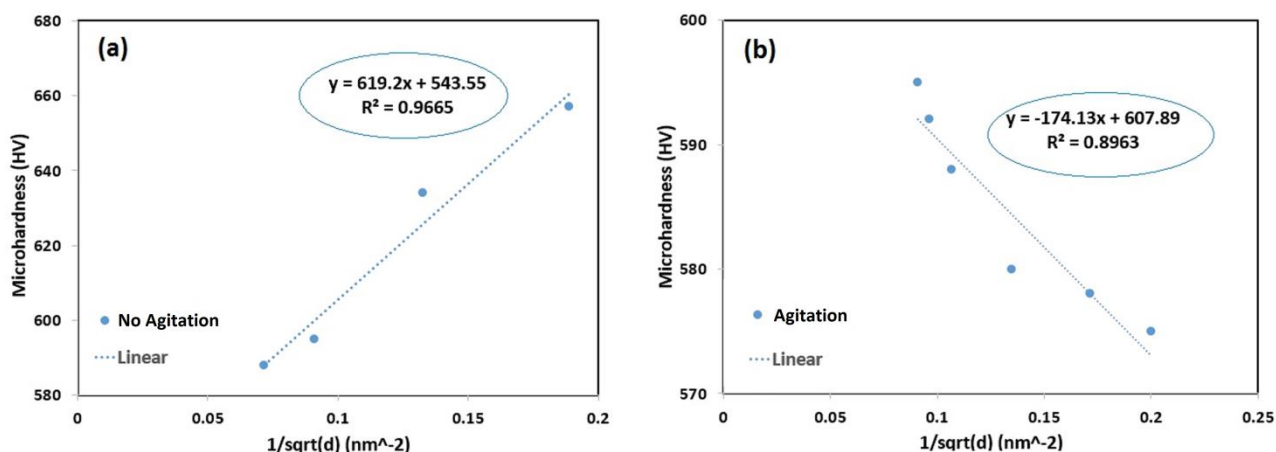


Figure 7. The Hall-Petch relationship at different current densities without agitation in the solution (a) and at different stirring rates in the solution (b).

Fig. 8 (b) illustrated the consequence of agitation on microhardness of the nanocrystalline pure nickel coating. Fig. 8 (b) indicated the aftermath of the stirring rates on the hardness of the nanocrystalline pure nickel coating. Maybe the formation of hollow bubbles on the cathode surface was the reason for this phenomenon although the increase of stirring rate led into finer crystallite size. Moreover, the hardness decreased, so this phenomenon was in conflict with Hall-Petch Theory.

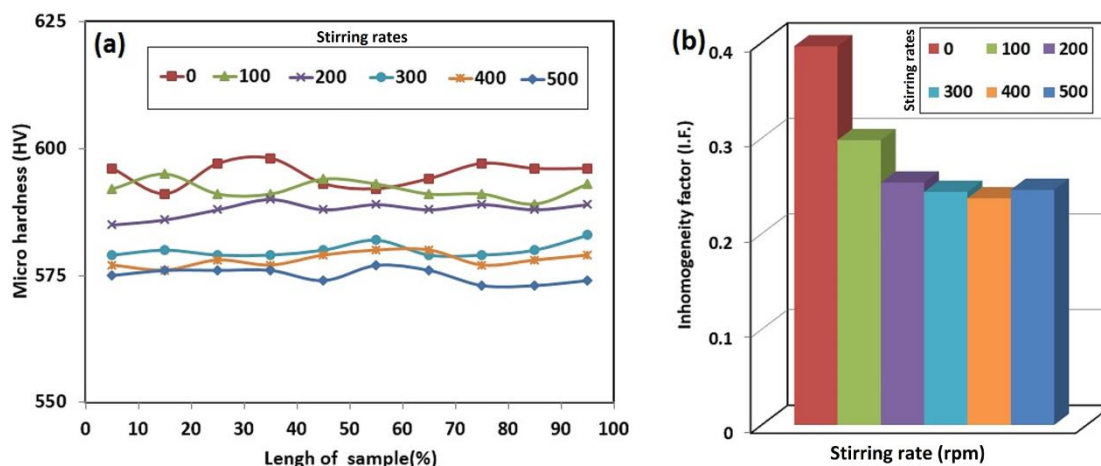


Figure 8. (a) The microhardness profile along the length of the specimen. (b) The variation of I.F. at different stirring rates in the solution.

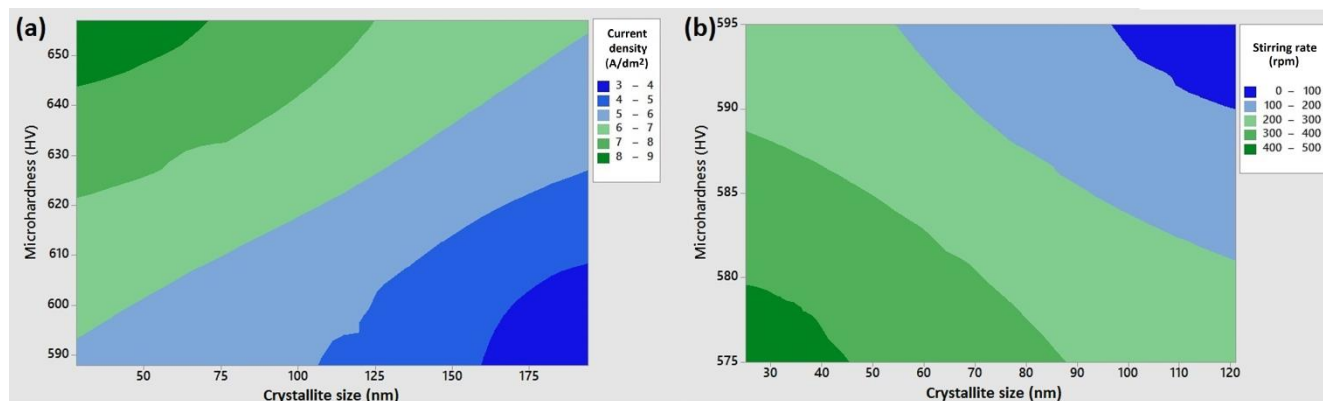


Figure 9. Contour plot of microhardness and crystallite size at (a) different current densities with no agitation in the system, (b) different stirring rates at 5 A/dm² current density.

Also, Fig. 9 (a) implied the effects of current density, microhardness and crystallite size on specimens with stationary bath. Increasing the crystallite size deteriorated the material mechanical properties. However, higher current density reinforced the structure and transferred it to higher microhardness values. Another unified presentation was Fig. 9 (b) which illustrated the stirring rate effects on microhardness and crystallite size. The notable point of these presentations was that higher and lower microhardness values (dark-green and dark-blue zones) were just centralized in specific regions of the plots. Accordingly, there was a logical correlation between parameters. The turbulence in the bath made finer crystallite size that did not improve the mechanical properties (even had a

damaging effect on it). This could be due to microstructure formation evolutions like the presence of cracks, blisters, and stresses effects. Therefore, higher crystallite size was achieved in specimens undergone lesser turbulence in the bath and also coated with higher current densities. Also, higher mechanical properties were achieved in the samples without agitation in the electroplating bath.

4. CONCLUSION

Eventually, the consequences of varying the current density and stirring rate of electroplating process on crystallite size, mechanical properties and corrosion behavior of nanocrystalline pure nickel coating were evaluated. Principal conclusions of this paper are imparted in the following expressions:

1. Crystallite size had an indirect relation with increasing the current density and high stirring rate. The least crystallite size of nickel coating achieved in this study was 28 nm at the current density of 5 A/dm² and 500 rpm stirring rate.

2. The agitation of the solution bath did not have a significant effect on the corrosion resistance of nanocrystalline nickel coating although agitation had an effect on corrosion current of the coating that the changes did not make a barrier against corrosion process.

3. In order to minimize the consumed energy, applying lowest optimum current density and stirring rate in the electroplating bath was recommended which would save the forming proper and fine crystalline structure. The 5 A/dm² current density and stirring rate with the maximum amount of 400 rpm can be used for affordable production.

4. Agitation in the bath solution led into homogeneous microhardness on the coating profile. The optimum stirring rate with most homogeneous hardness distribution was 400 rpm. Higher stirring rates affected the hardness distribution profile of the nanocrystalline nickel coating.

5. The relationship between crystallite size and microhardness of the nanocrystalline nickel coating in a stationary bath was in compliance with the Hall-Petch equation. However, agitation of the solution affected on the microhardness of the coating. Indeed, the higher stirring rate extenuated the microhardness of the coating which is not in agreement with the Hall-Petch relationship.

References

1. M. A. Meyers, A. Mishra and D. J. Benson, *Prog. Mater. Sci.*, 51 (2006) 427.
2. M. Aliofkhazraei, *Nanocoatings: size effect in nanostructured films*, Springer Science & Business Media, Springer, (2011) Berlin Heidelberg, Germany.
3. S. C. Tjong and H. Chen, *Mater. Sci. Eng. R.*, 45 (2004) 1.
4. Y. W. Song, D. Y. Shan and E. H. Han, *Mater. Lett.*, 62 (2008) 3276.
5. A. Salimi, E. Sharifi, A. Noorbakhsh and S. Soltanian, *Biosens. Bioelectron.*, 22 (2007) 3146.
6. A. M. Rashidi and A. Amadeh, *Surf. Coat. Tech.*, 202 (2008) 3772.
7. A. P. Malshe, W. Jiang and A. R. Dhamdhere, *JOM.*, 54 (2002) 28.
8. Z. J. Tian, D. S. Wang, G. F. Wang, L. D. Shen, Z. D. Liu and Y. H. Huang, *T. Nonfer. Metal. Soc.*, 20 (2010) 1037.
9. D. H. Jeong, F. Gonzalez, G. Palumbo, K. T. Aust and U. Erb, *Scripta Mater.*, 44 (2001) 493.
10. J. Sudagar, J. Lian and W. Sha, *J. Alloy. Compd.*, 571 (2013) 183.
11. A. Zarebidaki, H. Mahmoudikohani and M. R. Aboutalebi, *J. Alloy. Compd.*, 615 (2014) 825.
12. N. P. Wasekar, P. Haridoss, S. K. Seshadri and G. Sundararajan, *Wear.*, 296 (2012) 536.

13. C. Ma, S. C. Wang and F. C. Walsh, *T. I. Met. Finish.*, 93 (2015) 8.
14. R. Mishra and R. Balasubramaniam, *Corrosion. Sci.*, 46 (2004) 3019.
15. S. Mohan, S. Shriram and S. Karthikeyan, *Bull. Electrochem.*, 18 (2002) 241.
16. T. Kolonits, P. Jenei, B. G. Tóth, Z. Czigany, J. Gubicza, L. Peter and I. Bakonyi, *J. Electrochem. Soc.*, 163 (2016) 107-.
17. I. Gurrappa and L. Binder, *Sci. Tech. Adv. Mater.*, 9 (2008) 043001.
18. F. Ebrahimi and Z. Ahmed, *J. Appl. Electrochem.*, 33 (2003) 733.
19. K. L. Morgan, Z. Ahmed and F. Ebrahimi, *MRS. Online. P. Libr. Arch.*, 634 (2000) 3.
20. J. X. Kang, W. Z. Zhao and G. F. Zhang, *Surf. Coat. Tech.*, 203 (2009) 1815.
21. A. Cziraki, B. Fogarassy, I. Gerocs, E. Toth-Kadar and I. Bakonyi, *J. Mater. Sci.*, 29 (1994) 4771.
22. R. Sen, S. Das and K. Das, *J. Nanosci. Nanotechnol.*, 10 (2010) 8217.
23. A. Ciszewski, S. Posluszny, G. Milczarek and M. Baraniak, *Surf. Coat. Tech.*, 183 (2004) 127.
24. O. Sadiku-Agboola, E. R. Sadiku and O. F. Biotidara, *Inter. J. Phys. Sci.*, 7 (2012) 349.
25. Y. Nakamura, N. Kaneko, M. Watanabe and H. Nezu, *J. Appl. Electrochem.*, 24 (1994) 227.
26. L. Qin, J. Xu, J. Lian, Z. Jiang and Q. Jiang, *Surf. Coat. Tech.*, 203 (2008) 142.
27. A. M. Rashidi and A. Amadeh, *J. Mater. Sci. Tech.*, 26 (2010) 82.
28. M. Holm and T. J. Okeefe, *J. Appl. Electrochem.*, 30 (2000) 1125.
29. A. A. Rasmussen, P. Moller and M. A. J. Somers, *Surf. Coat. Tech.*, 200 (2006) 6037.
30. M. Stroumbouli, P. Gyftou, E. A. Pavlatou and N. Spyrellis, *Surf. Coat. Tech.*, 195 (2005) 325.
31. E. Moti, M. H. Shariat and M. E. Bahrololoom, *Mater. Chem. Phys.*, 111 (2008) 469.
32. Z. Zhu, D. Zhu, N. Qu and W. Lei, *Mater. Design.*, 28 (2007) 1776.
33. L. Benea, P. L. Bonora, A. Borello and S. Martelli, *Wear.*, 249 (2001) 995.
34. T. G. Nieh and J. G. Wang, *Intermetallics.*, 13 (2005) 377.
35. L. Wang, J. Zhang, Y. Gao, Q. Xue, L. Hu and T. Xu, *Scripta. Mater.*, 55 (2006) 657.
36. R. Sen, S. Das and K. Das, *Surf. Coat. Tech.*, 205 (2011) 3847.
37. S. K. Kim and H. J. Yoo, *Surf. Coat. Tech.*, 108 (1998) 564.
38. A. Conde, M. Arenas and J. De Damborenea, *Corrosion. Sci.*, 53 (2011) 1489.
39. G. Wu, N. Li, D. Zhou and K. Mitsuo, *Surf. Coat. Tech.*, 176 (2004) 157.
40. M. Vaezi, S. Sadrnezhaad and L. Nikzad, *Colloid. Surface. A.*, 315 (2008) 176.
41. P. Baghery, M. Farzam, A. Mousavi and M. Hosseini, *Surf. Coat. Tech.*, 204 (2010) 3804.
42. G. Palumbo, U. Erb and K. T. Aust, *Scr. Metall. Mater.*, 24 (1990) 2347.
43. A. H. Chokshi, A. Rosen, J. Karch and H. Gleiter, *Scripta. Metal. Mater.*, 23 (1989) 1679.
44. H. Zhao, L. Liu, J. Zhu, Y. Tang and W. Hu, *Mater. Lett.*, 61 (2007) 1605.
45. C. Cheung, G. Palumbo and U. Erb, *Scripta. Metal. Mater.*, 31 (1994) 735.
46. Y. Dong, P. Lin and H. Wang, *Surf. Coat. Tech.*, 200 (2006) 3633.